nature physics

LETTERS

https://doi.org/10.1038/s41567-019-0478-8

Stern–Gerlach detection of neutral-atom qubits in a state-dependent optical lattice

Tsung-Yao Wu, Aishwarya Kumar, Felipe Giraldo and David S. Weiss*

Qubit state measurements are an essential part of any quantum computer, constituting the readout. Accurate measurements are also an integral component of one-way quantum computation and of error correction, which is needed for fault-tolerant quantum computation[1]. Here, we present a state measurement for neutral-atom qubits based on coherent spatial splitting of the atoms' wavefunctions. It is reminiscent of the Stern–Gerlach experiment[2], but carried out in light traps. For around 160 qubits in a three-dimensional array, we achieve a measurement fidelity of 0.9994, which is roughly 20 times lower error than in previous measurements of neutral-atom arrays[3,4]. It also greatly exceeds the measurement fidelity of other arrays with more than four qubits, including those with ion and superconducting qubits[5,6]. Our measurement fidelity is essentially independent of the number of qubits measured, and since the measurement causes no loss, we can reuse the atoms. We also demonstrate that we can replace atoms lost to background gas collisions during the experiment[7].

Neutral atoms are promising qubit candidates, because they are identical, have long coherence times, and can be readily scaled to large arrays with spacings of several micrometres so that they can be individually addressed[8]. A simple way to measure the states of atom qubits is to resonantly push (clear) atoms in one qubit state out of the trap with light and detect those that remain. The detection fidelity for the remaining atoms can exceed 0.9997 (ref. [9]), but the scheme suffers from two considerable drawbacks. First, qubit loss during the computation is indistinguishable from the atom being in the cleared state, making the loss rate the de facto limit on the fidelity of the state measurement. Second, about half the atoms are cleared during measurement, necessitating reloading of atoms, thus making it hard to adapt this method to error correction. A few alternative approaches have been used to achieve lossless state detection. Atoms in each state can in turn be made to fluoresce on a cycling transition[3,4,10,11]. However, since the atoms cannot be cooled during the measurement, this method is a balance between detecting enough photons to identify the atom's state and those photons heating the atom out of the trap. The best results on small, 1D alkali-atom ensembles have had 0.987 fidelity and 2% heating loss[3] or 0.98 fidelity and 1% heating loss[4]. One-dimensional arrays of alkaline earth atoms have achieved 0.98 fidelity, limited by off-resonant scattering of trap light, with 0.5% heating loss[12]. Photon collection efficiency improves when a single atom is trapped in a high-finesse cavity[13,14], where 0.9992 fidelity has been achieved[14], but this enhancement is hard to scale to more atoms. In a quantum gas microscope, a large magnetic field gradient was applied to coherently separate atoms in two different internal states, reminiscent of the Stern–Gerlach experiment, after which the two states were trapped and detected at adjacent lattice sites[15]. A fidelity of 0.98 was reached, limited by lattice phase fluctuations. Our technique is also a Stern–Gerlach-type approach, but without magnetic field gradients.

Our state detection scheme is conceptually illustrated in Fig. 1a. We start with atoms in a 3D lattice with a large spacing in all directions (lattice XYZ) in an unknown superposition of two internal states. To detect the state of each atom, we adiabatically transform the state-independent X lattice into two state-dependent potentials that move in opposite directions[7,16,17]. The two state components of each atom follow their respective potentials, spatially splitting the wavefunction in two. Next, we replace X with X_S, a lattice with an order of magnitude shorter lattice spacing. The two parts of the wavefunction are each localized to within a couple of X_S lattice sites. We then image the atoms with cooling light[9], which projects the wavefunction of each atom onto a single site in X_SYZ, and measures its location. Mapping the internal state to spatial position in this way avoids the detection–heating trade-off that has limited previous measurements.

The X, Y and Z lattices in our experiment are created by pairs of 839 nm laser beams, crossing at 10° angles as shown in Fig. 1b, linearly polarized perpendicular to their plane of propagation. The lattice beams are slightly mutually shifted in frequency (by tens of megahertz), and together form an approximately cubic 3D lattice with 4.8 μm spacing and 190 μK depth. The vibrational frequency of an atom trapped near the bottom of a lattice site is 15 kHz (ref. [9]). Caesium atoms are loaded into the lattice from a magneto-optic trap. We can either use the approximately 40% random occupancy we start with, or sort atoms to fully fill a sublattice[7]. We detect atoms in five planes by imaging phase-scrambled (see Supplementary Information) polarization gradient cooling light one Z plane at a time, which takes 830 ms in total (see Supplementary Information). Projection sideband cooling[7,18] leaves 89% of the atoms in their 3D vibrational ground states and more than 99.9% of the atoms in the $|F=4,m_F=-4\rangle$ hyperfine ground state, where F and m_F are the hyperfine and magnetic quantum numbers, respectively. We can transfer atoms into any other magnetic sublevel with a series of adiabatic fast passage (AFP) microwave pulses[19], and we can create superpositions of sublevels using Blackman pulses[19].

The 3D lattice initially traps all hyperfine sublevels nearly identically (see Fig. 1a (i)). We make the X lattice sublevel-dependent by rotating the polarization of one of its beams, which we accomplish with two Pockels cells and a $\lambda/4$ plate[7]. Atoms in different hyperfine levels with the same sign of m_F, such as $|F=4,m_F=-4\rangle$ and $|F=3,m_F=-3\rangle$, move in opposite directions. A nearly $\pi/2$ polarization rotation separates the two states by almost half the X lattice spacing (see Fig. 1a (ii)). Ramping the voltage on the Pockels cell within 300 μs keeps the motion adiabatic. At the end of the ramp we suddenly turn on a retro-reflected approximately 150 μm waist laser beam that forms a lattice, X_S, with 0.42 μm spacing (see Fig. 1b and Fig. 1a (iii)). To avoid mutual interference, the wavelength of the X_S

Physics Department, Pennsylvania State University, University Park, PA, USA. *e-mail: dsweiss@phys.psu.edu

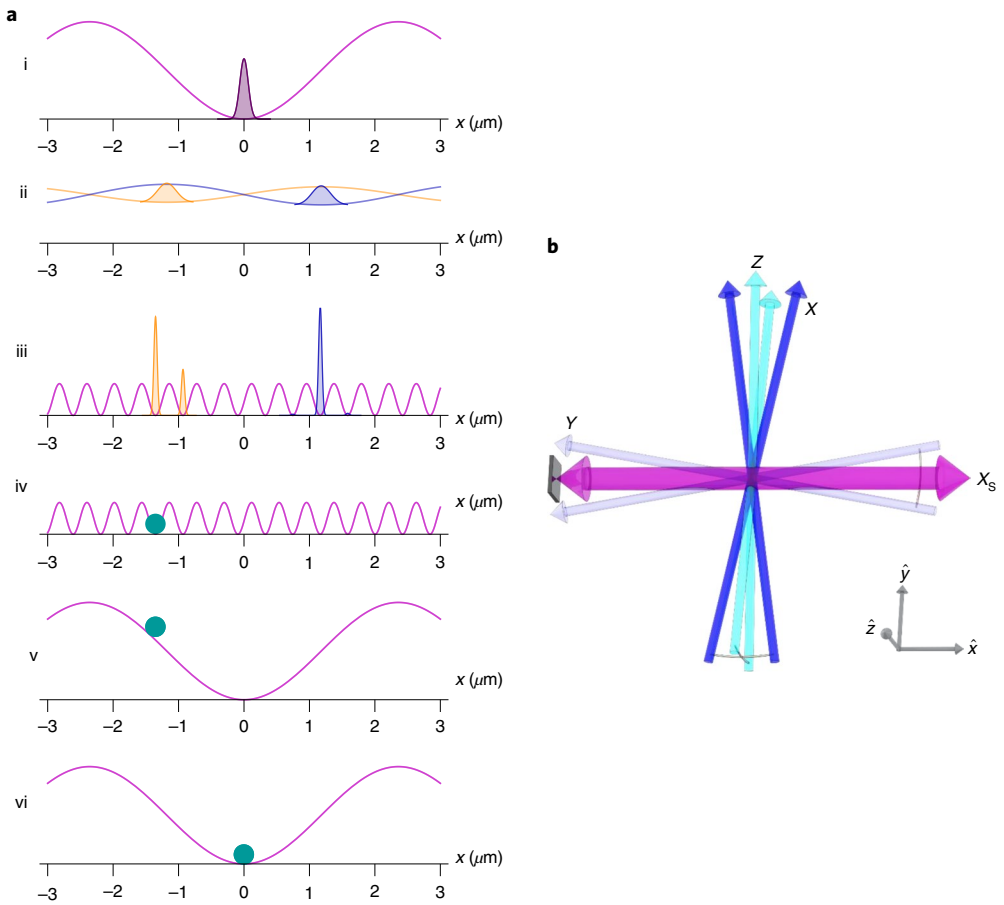

Fig. 1 | Overview of lossless state detection. a, State detection steps. The potential energy curves have a consistent vertical scale and the atomic wavefunctions are normalized. (i), Pre-measurement state. The purple curve denotes the state-independent potential energy in the *x* direction (*X* lattice). The purple shaded region represents the wavefunction of an atom in the vibrational ground state and an equal superposition of two states. (ii), Displaced state-dependent lattices. The potential has been adiabatically transformed into two shallower state-dependent potentials, where the potential energy and wavefunction for each of the two states are shown in orange and blue. (iii), Transfer atoms to X_S. For each internal state, the number of X_S lattice sites with substantial wavefunction amplitude depends on the relative position of the X_S and the state-dependent *X* potential energy minima, which are not fixed in our experiment. (iv), Image atoms in X_S. The wavefunction has been projected onto a single lattice site. The atom, now spread among many internal states and several vibrational levels, is denoted by the cyan circle. Its location is used for state assignment. (v), Atom transferred back to *X*. (vi), Atom at the bottom of *X* after one quarter oscillation period. At this point, another image is taken. **b**, Diagram of the lattice beams. The *X*, *Y* and *Z* lattices consist of pairs of linearly polarized laser beams crossing at 10° angles (drawn as 20° in the figure, but otherwise to scale), giving 4.8 μm lattice spacings. The beams are focused at the atoms with a Gaussian waist of 75 μm. The X_S lattice (purple with double arrows) is formed by retro-reflection, resulting in a 0.42 μm lattice spacing. The X_S beam has an approximately 150 μm Gaussian waist at the atoms.

light is slightly different (by tens of megahertz) from the other lattice beams. The spatial phase of X_S relative to *X* is not controlled. After the initial turn on, the X_S power is increased within 78 μs so that the vibrational frequency in the ground state is raised from 43 kHz to 98 kHz, a sequence empirically adjusted to avoid site hopping in X_S. We then turn off *X* and turn on the polarization gradient cooling light to cool and image the atoms. The wavefunction of the atom is thus projected into a single site of the $X_S YZ$ lattice (see Fig. 1a (iv)).

In Fig. 2a we show the results of measurements starting with all atoms in $|F=4, m_F=-4\rangle$ after optical pumping. For Fig. 2b, the atoms start in $|F=3,m_F=-3\rangle$ after an AFP pulse and an $F=4$ state-clearing laser pulse to ensure clean state preparation. The single plane images are typical and the grid vertices demark the initial atom locations. The detected atoms are clearly shifted to the left for $|F=4,m_F=-4\rangle$ and to the right for $|F=3,m_F=-3\rangle$. The locations of the atoms are fitted to a floating *x* centre (see Supplementary Information), and the distributions of these positions are shown in the histograms, which quantify the qualitative shifts visible in the images. For Fig. 2c, the atoms start in a superposition of the two internal states. We set the line that separates atoms in the two states at −0.2 μm, equidistant from the two peaks, and colour the histograms and the occupancy maps accordingly.

The Gaussian root-mean-square widths of the displacement distributions in Fig. 2 are 203 nm, which is about half an X_S lattice spacing (210 nm). This width mostly results from the random phase relationship between *X* and X_S. We infer that the asymmetry of the displacement centres results from slight imperfections in the *X* polarization (see Supplementary Information). Across the entire 9×9×5 array, $7^{+4}_{-3}\times10^{-4}$ of the atoms nominally prepared in $|F=4,m_F=-4\rangle$ are measured to be in $|F=3,m_F=-3\rangle$ and $5^{+3}_{-2}\times10^{-4}$ of the atoms nominally prepared in $|F=3,m_F=-3\rangle$ are measured to be in $|F=4,m_F=-4\rangle$ (see insets of Fig. 2a,b), yielding an average state detection fidelity of 0.9994.

When atoms spontaneously emit lattice light before they are captured in X_S, they can change state and move in the wrong direction. We calculate a scattering rate of 3×10^{-4} during the motion in *X*,

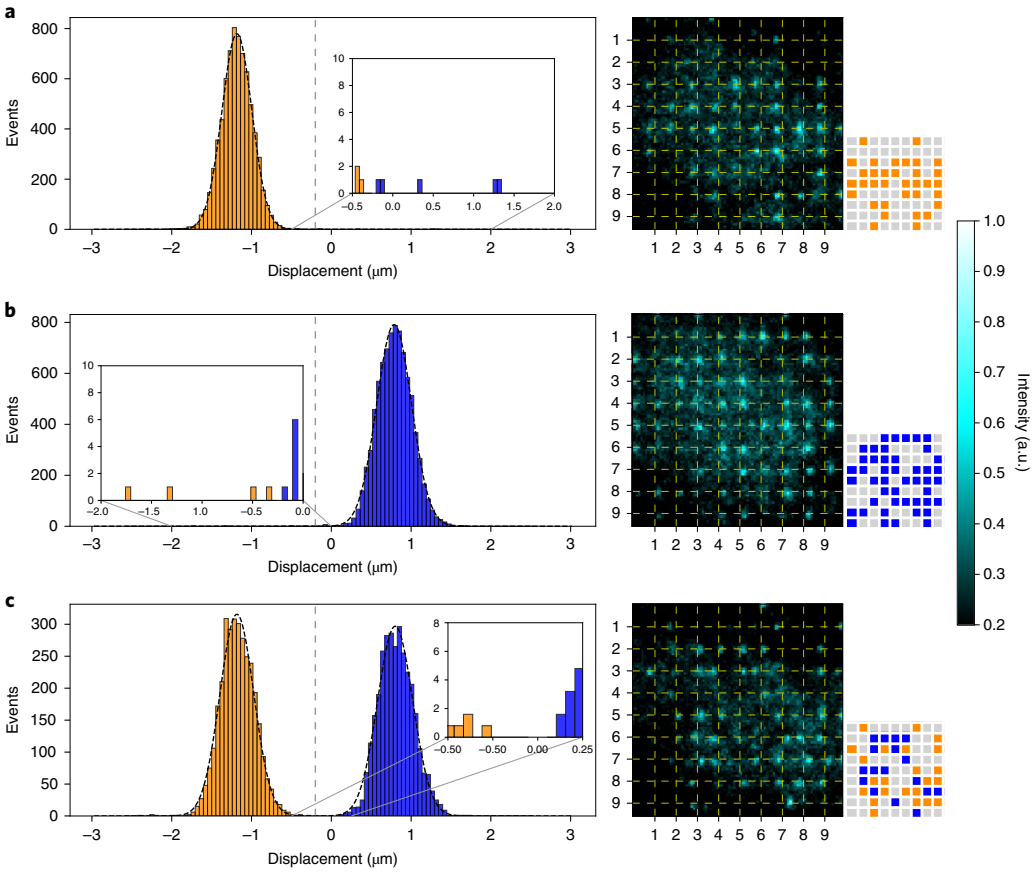

Fig. 2 | Displacement distributions and state assignment. The histograms show the displacement distributions during state detection. The atom centres are fitted to within a 0.15 μm s.d. (see Supplementary Information) and the 0.05 μm bin width is chosen to be small enough that no spatial information is lost. **a**, Atoms prepared in $|F=4,m_F=-4\rangle$. **b**, Atoms prepared in $|F=3,m_F=-3\rangle$. **c**, Atoms prepared in a superposition state. For each histogram we performed 50 implementations starting with a 30–40% randomly loaded 9×9×5 lattice. The black dashed lines are Gaussian fits to the distributions. The vertical grey dashed line at −0.2 μm sets the dividing line for state assignment. Atoms to the left (right) are ascribed to $|F=4,m_F=-4\rangle$ ($|F=3,m_F=-3\rangle$) and coloured orange (blue). The state detection errors, those events that are nominally prepared in one state but are detected in the other state, are highlighted in the insets of **a** and **b**. The inset of **c** is a magnified histogram of the intermediate displacement region. An example image of one lattice plane is shown next to each histogram. The colour scale to the right is the intensity key, which uses contrast enhancement. The displacement of each atom in the *x* direction (horizontal in the image) is the difference between its fit centre and its initial position, which is marked by the dashed yellow grid. The occupancy map for each example image is shown in the associated square pattern. Orange or blue denotes an occupied site in one of the two states, while grey represents an empty site.

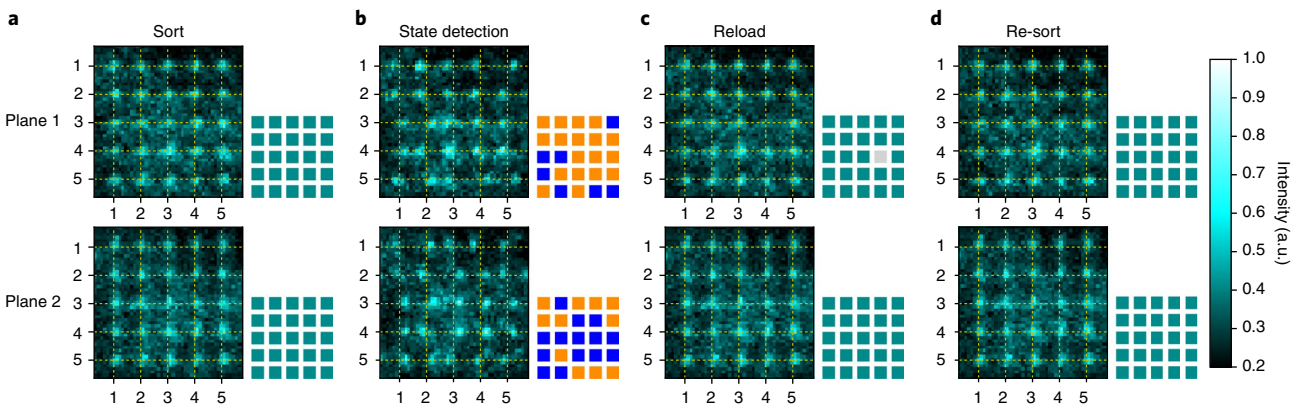

Fig. 3 | Demonstration of re-initialization of a 3D qubit array. The two images in each column correspond to different lattice planes. The colour scale to the right is the intensity key, which has contrast enhancement. The dashed yellow grid marks the initial atom locations. The associated square patterns show the occupancy maps. Cyan denotes an occupied *XYZ* site, orange and blue denote an atom determined to be in the $|F=4,m_F=-4\rangle$ and $|F=3,m_F=-3\rangle$ state, respectively, and grey denotes an empty site. **a**, Perfect filling of a 5×5×2 array after sorting from a randomly half-filled 5×5×5 *XYZ* lattice. **b**, Lossless state detection in X_SYZ after the atoms were prepared in an equal superposition of $|F=4,m_F=-4\rangle$ and $|F=3,m_F=-3\rangle$. **c**, Atoms reloaded into *XYZ*. Note that an atom in plane 1 (at (4, 3)) has been lost owing to a background gas collision. **d**, Re-sorted atoms. The vacancy has been filled with an atom from the reservoir region (outside these two planes but within 5×5×5), where extra atoms had been left during the initial sorting.

which is consistent with this being the dominant source of error. If the X polarization were to be improved, we could move the atoms faster and thus reduce the scattering and the associated state detection error. We could also employ a 'throw and catch' method. In this scheme, we would suddenly change an X beam polarization, let the atoms be accelerated by the shifted lattices, and then shut off X to avoid spontaneous emission. When the atoms have travelled sufficiently far, X_S would be turned on with cooling light to catch the atoms. We estimate that this could reduce our error from spontaneous emission by a factor of five.

After the state measurement, we adiabatically turn X back on with its standard polarization and then turn off X_S with essentially the reverse sequence that we used to turn it on (see Fig. 1a (v) and Supplementary Information). One quarter oscillation cycle later, when the atoms are centred in X (see Fig. 1a (vi)), we recool them and take another set of pictures to determine the final occupancy. The final occupancy map facilitates the occupancy determination in X_SYZ, bringing its error below 10^{-4} (see Supplementary Information). Between the initial occupancy determination and the state detection, 2% of the atoms are lost, which is consistent with independent measurements of the loss rate due to collisions with the background gas. We infer that the state detection measurement itself causes no loss. We also see no evidence of loss or site hopping due to the process of transferring the atoms back to X.

With essentially lossless detection, we can re-initialize our qubits after state measurement, a procedure we demonstrate in Fig. 3. We first sort to get a perfectly filled $5\times5\times2$ pattern (see Fig. 3a)[7]. We then prepare an equal superposition of the two stretched states, execute state detection in X_SYZ (see Fig. 3b), and reload into XYZ (see Fig. 3c). Atom loss to a background gas collision can occur in either stage; in this implementation, one atom was lost between state detection and reloading. We re-sort, filling the vacancy with an atom from the reservoir region (within $5\times5\times5$ but outside $5\times5\times2$) (see Fig. 3d). The ability to fix qubit loss errors will ultimately be an important element of quantum error correction.

Because of their insensitivity to noise, it is preferable to quantum compute in the clock states, $|F=4,m_F=0\rangle$ and $|F=3,m_F=-0\rangle$ (ref. [20]). However, these states do not move in the state-dependent lattice. To generalize our detection method, we use two AFP pulses to transfer atoms from superpositions of clock states to superpositions of $|F=4,m_F=-2\rangle$ and $|F=3,m_F=-2\rangle$, and detect the state from there (see Supplementary Information). We generate a range of clock state superpositions by transferring all the atoms to $|F=3,m_F=0\rangle$ and executing a $\pi/2$–π–π–$\pi/2$ sequence on the clock transition, scanning the phase of the final pulse. We do this in a one-quarter-depth XYZ lattice, which is preferred for minimizing decoherence while maintaining gate fidelity. Before state detection, we adiabatically raise the lattice to full power. The result is shown in Fig. 4a, with 480 μs between the $\pi/2$ pulses. The fraction of atoms found in the wrong state at phase π is $0^{+5}_{-0}\times10^{-4}$, which is to say we found no errors in 2,200 atom detections, consistent with as good a fidelity as we measured starting from the stretched states. The error at phase 0 is larger, $22^{+12}_{-8}\times10^{-4}$. We attribute the poorer performance when measuring from the $|F=4,m_F=0\rangle$ state to Rabi frequency differences between the various AFP microwave transitions (see Supplementary Information). Adding the ability to dynamically change the microwave polarization should avoid this issue completely.

To further make use of our state detection method, we measure our qubit coherence time by adding additional intermediate π pulses at 20 ms intervals (see Supplementary Information) and performing the spin-echo measurement described above with longer evolution times. From the observed fringe contrast as a function of time, shown in Fig. 4b, we find that the coherence times (T_2' and T_1) for atoms in a $5\times5\times5$ volume is 12.6 s. The improvement over our previously reported coherence time of 7.4 s (refs. [7,19]) results from

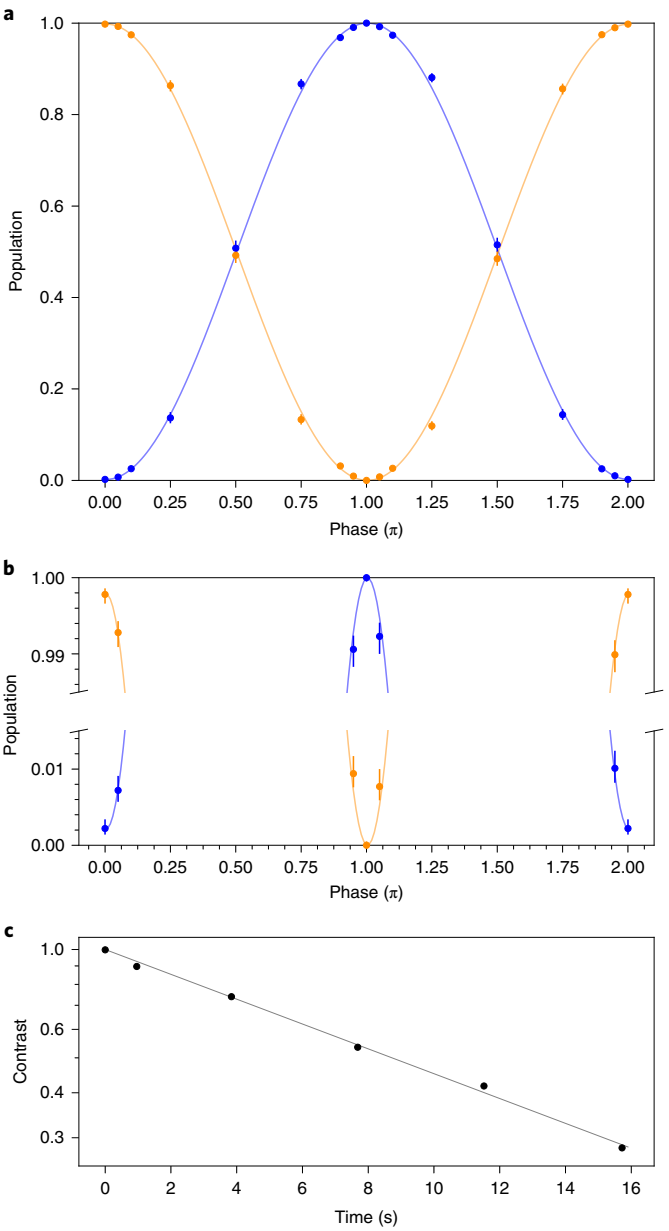

Fig. 4 | State-selective detection from the clock states. a, Fringes from a spin-echo measurement sequence on the $|F=4,m_F=0\rangle$ and $|F=3, m_F=0\rangle$ transition. The evolution time is 480 μs and the phase of the final $\pi/2$ pulse is scanned. Atoms are transferred with microwave AFP pulses to $|F=4,m_F=-2\rangle$ (orange) and $|F=3,m_F=-2\rangle$ (blue) for state detection. At each point, the populations of both states are determined in the same state measurement. The data points at phase 2π are the same as those at phase 0. The solid curves are fits using a sine function, and the fit amplitude gives the fringe contrast. **b**, Magnified regions of **a**. At phases π and 0, perfect state preparation and detection would lead to all atoms being in the same state. At π phase, there were no errors among the 2,200 atoms we measured. We attribute the 2×10^{-3} error at 0 phase to the lower quality of some AFP pulses (see Supplementary Information). Error bars in **a** and **b** represent 1 s.d. and are due to counting statistics. The error bars for the data points at phase π are smaller than the size of the symbols. **c**, Semi-logarithmic plot of fringe contrasts for spin-echo sequences, for a range of evolution times. The fitted exponential time constant, which gives the coherence time of the qubits, is 12.6 s. The one standard deviation error bars from the fringe contrast fits are smaller than the size of the symbols.

better cooling and a farther-detuned optical lattice, both of which minimize spontaneous emission from the lattice.

The concept of our state measurement method, where internal states are mapped to atom positions, can be generalized to atoms in reconfigurable dipole-trap arrays[21–24]. Each dipole trap can be formed by overlapping two traps with opposite circular polarization. For state detection, the two traps can be spatially separated. If needed, dipole heating could be minimized by making the two traps linearly polarized before the atoms are imaged.

While it can now be used for final state readout, we ultimately plan to adapt this measurement technique to quantum error correction, where state detection of only a subset of the atoms is required[25–27]. The atoms to be detected would be selectively transferred to larger m_F states. During the motion, the clock state qubits will remain weakly trapped at their original position. Transferring them to X_S will probably require matching the nodes of X to nodes of X_S. Speed concerns will require fluorescent detection to be replaced with phase-contrast imaging[28], which would act as a form of holography and allow all planes to be imaged at once. Preventing the undetected qubits from interacting with detection light will require the qubits to be shifted out of resonance or transferred to dark states, or the use of a second atomic species for measurement[29]. Our state detection error approaches the commonly accepted threshold of 10^{-4} for fault-tolerant quantum computation[30], and it already comfortably surpasses the thresholds of about 10^{-3} used for some surface codes[31].

Data availability

The data that support the plots in this paper are available from the corresponding author upon reasonable request.

Received: 31 August 2018; Accepted: 18 February 2019;
Published online: 25 March 2019

References

1. Bruss, D. & Leuchs, G. *Lectures on Quantum Information* (Wiley, 2007).
2. Gerlach, W. & Stern, O. *Der experimentelle Nachweis der Richtungsquantelung im Magnetfeld. Z. Phys.* **9**, 349–352 (1922).
3. Kwon, M., Ebert, M. F., Walker, T. G. & Saffman, M. Parallel low-loss measurement of multiple atomic qubits. *Phys. Rev. Lett.* **119**, 180504 (2017).
4. Martinez-Dorantes, M. et al. Fast nondestructive parallel readout of neutral atom registers in optical potentials. *Phys. Rev. Lett.* **119**, 180503 (2017).
5. Debnath, S. et al. Demonstration of a small programmable quantum computer with atomic qubits. *Nature* **536**, 63–66 (2016).
6. Jeffrey, E. et al. Fast accurate state measurement with superconducting qubits. *Phys. Rev. Lett.* **112**, 190504 (2014).
7. Kumar, A., Wu, T.-Y., Giraldo Mejia, F. & Weiss, D. S. Sorting ultracold atoms in a 3D optical lattice in a realization of Maxwell's demon. *Nature* **561**, 83–87 (2018).
8. Weiss, D. & Saffman, M. Quantum computing with neutral atoms. *Phys. Today* **70**, 45–50 (2017).
9. Nelson, K. D., Li, X. & Weiss, D. S. Imaging single atoms in a three-dimensional array. *Nat. Phys.* **3**, 556–560 (2007).
10. Gibbons, M. J., Hamley, C. D., Shih, C. Y. & Chapman, M. S. Nondestructive fluorescent state detection of single neutral atom qubits. *Phys. Rev. Lett.* **106**, 133002 (2011).
11. Fuhrmanek, A., Bourgain, R., Sortais, Y. R. P. & Browaeys, A. Free-space lossless state detection of a single trapped atom. *Phys. Rev. Lett.* **106**, 133003 (2011).
12. Covey, J. P., Madjarov, I. S., Cooper, A. & Endres, M. 2000-times repeated imaging of strontium atoms in clock-magic tweezer arrays. Preprint at https://arxiv.org/abs/1811.06014 (2018).
13. Bochmann, J. et al. Lossless state detection of single neutral atoms. *Phys. Rev. Lett.* **104**, 203601 (2010).
14. Gehr, R. et al. Cavity-based single atom preparation and high-fidelity hyperfine state readout. *Phys. Rev. Lett.* **104**, 203602 (2010).
15. Boll, M. et al. Spin- and density-resolved microscopy of antiferromagnetic correlations in Fermi-Hubbard chains. *Science* **353**, 1257–1260 (2016).
16. Deutsch, I. H. & Jessen, P. S. Quantum-state control in optical lattices. *Phys. Rev. A* **57**, 1972–1986 (1998).
17. Robens, C. et al. Low-entropy states of neutral atoms in polarization-synthesized optical lattices. *Phys. Rev. Lett.* **118**, 065302 (2017).
18. Li, X., Corcovilos, T. A., Wang, Y. & Weiss, D. S. 3D projection sideband cooling. *Phys. Rev. Lett.* **108**, 103001 (2012).
19. Wang, Y., Zhang, X. L., Corcovilos, T. A., Kumar, A. & Weiss, D. S. Coherent addressing of individual neutral atoms in a 3D optical lattice. *Phys. Rev. Lett.* **115**, 043003 (2015).
20. Wang, Y., Kumar, A., Wu, T. Y. & Weiss, D. S. Single-qubit gates based on targeted phase shifts in a 3D neutral atom array. *Science* **352**, 1562–1565 (2016).
21. Barredo, D., Lienhard, V., De Leseleuc, S., Lahaye, T. & Browaeys, A. Synthetic three-dimensional atomic structures assembled atom by atom. *Nature* **561**, 79–82 (2018).
22. Endres, M. et al. Atom-by-atom assembly of defect-free one-dimensional cold atom arrays. *Science* **354**, 1024–1027 (2016).
23. Kim, H. et al. In situ single-atom array synthesis using dynamic holographic optical tweezers. *Nat. Commun.* **7**, 13317 (2016).
24. Lester, B. J., Luick, N., Kaufman, A. M., Reynolds, C. M. & Regal, C. A. Rapid production of uniformly filled arrays of neutral atoms. *Phys. Rev. Lett.* **115**, 073003 (2015).
25. Schindler, P. et al. Experimental repetitive quantum error correction. *Science* **332**, 1059–1061 (2011).
26. Linke, N. M. et al. Fault-tolerant quantum error detection. *Sci. Adv.* **3**, e1701074 (2017).
27. Kelly, J. et al. State preservation by repetitive error detection in a superconducting quantum circuit. *Nature* **519**, 66–69 (2015).
28. Yamamoto, R. et al. Site-resolved imaging of single atoms with a Faraday quantum gas microscope. *Phys. Rev. A* **96**, 033610 (2017).
29. Saffman, M. Quantum computing with atomic qubits and Rydberg interactions: progress and challenges. *J. Phys. B* **49**, 202001 (2016).
30. Fowler, A. G., Mariantoni, M., Martinis, J. M. & Cleland, A. N. Surface codes: towards practical large-scale quantum computation. *Phys. Rev. A* **86**, 032324 (2012).
31. Raussendorf, R. & Harrington, J. Fault-tolerant quantum computation with high threshold in two dimensions. *Phys. Rev. Lett.* **98**, 190504 (2007).

Acknowledgements

This work was supported by US National Science Foundation grant numbers PHY-1520976 and PHY-1820849.

Author contributions

All authors contributed to the design, execution and analysis of the experiment and the writing of the manuscript. A.K., T.-Y.W. and F.G. collected all the data.

Competing interests

The authors declare no competing interests.

Additional information

Supplementary information is available for this paper at https://doi.org/10.1038/s41567-019-0478-8.

Reprints and permissions information is available at www.nature.com/reprints.

Correspondence and requests for materials should be addressed to D.S.W.

Publisher's note: Springer Nature remains neutral with regard to jurisdictional claims in published maps and institutional affiliations.